

Antimicrobial, antibiofilm, and anticancer potential of silver nanoparticles synthesized using pigment-producing *Micromonospora* sp. SH121

Birgöl Mazmancı, Serpil Könen Adıgöznel, Yiğit Süha Sadak, Derya Yetkin, Hilal Ay & Ali Osman Adıgöznel

To cite this article: Birgöl Mazmancı, Serpil Könen Adıgöznel, Yiğit Süha Sadak, Derya Yetkin, Hilal Ay & Ali Osman Adıgöznel (2022): Antimicrobial, antibiofilm, and anticancer potential of silver nanoparticles synthesized using pigment-producing *Micromonospora* sp. SH121, *Preparative Biochemistry & Biotechnology*, DOI: [10.1080/10826068.2022.2101001](https://doi.org/10.1080/10826068.2022.2101001)

To link to this article: <https://doi.org/10.1080/10826068.2022.2101001>



View supplementary material [↗](#)



Published online: 20 Jul 2022.



Submit your article to this journal [↗](#)



Article views: 37



View related articles [↗](#)



View Crossmark data [↗](#)

Antimicrobial, antibiofilm, and anticancer potential of silver nanoparticles synthesized using pigment-producing *Micromonospora* sp. SH121

Birgül Mazmanlı^{a,b}, Serpil Könen Adıgüzel^c, Yiğit Süha Sadak^b, Derya Yetkin^d, Hilal Ay^e, and Ali Osman Adıgüzel^e

^aDepartment of Nanotechnology and Advanced Material, Science Institute, Mersin University, Mersin, Turkey; ^bDepartment of Biology, Faculty of Science and Letter, Mersin University, Mersin, Turkey; ^cDepartment of Biology, Faculty of Science and Letter, Süleyman Demirel University, Isparta, Turkey; ^dFaculty of Science and Letter, Advanced Technology Education Research and Application Center, Süleyman Demirel University, Isparta, Turkey; ^eDepartment of Molecular Biology and Genetics, Faculty of Science and Letter, Ondokuz Mayıs University, Samsun, Turkey

ABSTRACT

Silver nanoparticles (AgNPs) have gained interest as an alternative pharmaceutical agent because of antimicrobial resistance and drug toxicity. Considering the increasing request, eco-friendly, sustainable, and cost-effective synthesis of versatile AgNPs has become necessary. In this study, green-made AgNPs were successfully synthesized using *Micromonospora* sp. SH121 (Mm-AgNPs). Synthesis was verified by surface plasmon resonance (SPR) peak at 402 nm wavelength in the UV-Visible (UV-Vis) absorption spectrum. Scanning electron microscopy (SEM) analysis depicted that Mm-AgNPs were in the size range of 10–30 nm and spherical. Fourier transform infrared spectroscopy (FTIR) confirmed the existence of bioactive molecules on the surface of nanoparticles. The X-ray diffraction (XRD) analysis revealed the face-centered cubic (fcc) structure of the Mm-AgNPs. Their polydispersity index (PDI) and zeta potential were 0.284 and –35.3 mV, respectively. Mm-AgNPs (4–32 µg/mL) exhibited strong antimicrobial activity against *Bacillus cereus*, *Enterococcus faecalis*, *Enterococcus hirae*, *Escherichia coli*, *Klebsiella pneumoniae*, *Proteus vulgaris*, *Pseudomonas putida*, *Staphylococcus epidermidis*, *Streptococcus pneumoniae*, and *Aspergillus flavus*. Mm-AgNPs partially inhibited the biofilm formation in *Acinetobacter baumannii*, *E. coli*, *K. pneumoniae*, and *Pseudomonas aeruginosa*. Furthermore, results showed that low concentrations of Mm-AgNPs (1 and 10 µg/mL) caused higher cytotoxicity and apoptosis in DU 145 cells than human fibroblast cells. Based on the results, Mm-AgNPs have an excellent potential for treating infectious diseases and prostate cancer.

KEYWORDS


Anticancer; antimicrobial activity; green-made silver nanoparticles; *Micromonospora* sp.; physicochemical characteristics

Introduction

Over the past few decades, antibiotic resistance (AR) in microorganisms has increased due to the unregulated and over-the-counter use of antibiotics. AR causes a socioeconomic burden for patients and governments due to increased morbidity, mortality, hospital stay, drug exposure, and treatment cost.^[1,2] According to the Centers for Disease Control and Prevention (CDC), complications of antibiotic-resistance infections (ARI) cause over 35,000 deaths each year. The United States Pharmacopeia (USP), an independent scientific organization, announced that if ARI is not prevented, deaths could reach 10 million per year by 2050.^[3] In addition, it has been estimated that ARI causes annual global economic losses exceeding 100 trillion dollars.^[4] Therefore, the demand for antibiotic alternatives has increased in recent years. Today, many studies have shown that silver nanoparticles (AgNPs) with unique properties

such as large surface area, high energy, and smoothness are suitable alternatives to antibiotics.^[5]

Cancer has known as another significant public health problem worldwide. In 2020, there was a significant decline in the diagnosis and treatment of cancer because of the coronavirus diseases 2019 (COVID-19) pandemic.^[6] In this case, it may lead to undesirable results such as increased mortality and advanced-stage disease. Prostate cancer has the highest incidence rate among older men (>65 years of age) and has become one of the most frequent malignancies after lung cancer.^[7] Radiation therapy is often preferred to treat most cancer patients. However, it may lead to adverse effects, including DNA damage and blocked cell division in normal cells.^[8] It is necessary to use new approaches for efficient treatment in cancer patients. Recently, studies related to the use in medicine (diagnosis and treatment) of nanoparticles synthesized by different routes have been raised. These studies have shown that nanoparticles are widely used to treat cancer.^[9,10]

CONTACT Ali Osman Adıgüzel  adiguzel.ali.osman@gmail.com  Department of Molecular Biology and Genetics, Faculty of Science and Letter, Ondokuz Mayıs University, Samsun, Turkey.

 Supplemental data for this article is available online at <https://doi.org/10.1080/10826068.2022.2101001>

© 2022 Taylor & Francis Group, LLC

AgNPs can be efficiently synthesized through chemical and physical methods. Chemical methods contain chemical reduction, sonochemical irradiation, electrochemical deposition, microemulsion, and so on.^[11,12] These methods threaten human health, occupational safety, and environmental sustainability as they require the use of toxic chemicals.^[13] On the other hand, physical methods including tube furnace, laser ablation, evaporation/condensation, ball milling, and pyrolysis are expensive, energy-intensive and time consuming.^[14] In addition, it is very difficult to adopt these methods to an industrial-scale. Therefore, developing the clean, easy to handle, cost-effective, and safe route for synthesizing AgNPs using biological methods involving compounds from plants, bacteria, fungi, and algae has recently received significant attention.^[15,16]

Bacteria are preferred in synthesizing AgNPs since they give a large amount of biomass in a short time without expensive and specific nutrients in an artificial environment. They produce various bioactive compounds that can be used as reducing and capping agents in extracellularly synthesizing AgNPs. Furthermore, the remaining biomass can be used to obtain high-value-added products such as pigments, proteins, enzymes, and antibiotics.^[17]

In the present study, green-made AgNPs were synthesized using culture supernatant of pigment-producing *Micromonospora* sp. SH121. Physicochemical properties of the synthesized AgNPs were revealed using SEM, EDS, FTIR, XRD, and zeta sizer. Afterward, their antimicrobial, antibiofilm, and DNA cleavage activities were investigated. Finally, cytotoxic, genotoxic, and apoptotic effects of the AgNPs on the prostate carcinoma cells and the normal human dermal fibroblasts cells were detected using the xCELLigence real-time cell analysis, comet assay, and Annexin V-PI assay, respectively.

Materials and methods

Material

Nutrient Agar (NA), Mueller-Hinton Agar (MHA), Mueller-Hinton Broth (MHB), peptone, glucose, malt extract, yeast extract, silver nitrate (AgNO₃), sodium hydroxide (NaOH), and 0.45 μL syringe filter were obtained from Merck (Darmstadt, Germany). Yeast Extract Peptone Dextrose Agar (YPDA) and Yeast Extract Peptone Dextrose Broth (YPDB) were purchased by MP Biomedicals (California, United States). Sulfuric acid (H₂SO₄) and hydrochloric acid (HCl) were supplied from Sigma-Aldrich (St. Louis, MO). Cell lines DU145 (ATCC[®] HTB-81[™]) and BJ-5ta (ATCC[®] CRL-4001[™]) were obtained from the American Type Culture Collection (ATCC). Cell line mediums were purchased from Biowest.

Synthesis of AgNPs

A loop of *Micromonospora* sp. SH121 colonies from ISP2 Agar (4 g/L glucose, 4 g/L yeast extract, 10 g/L malt extract, 20 g/L agar) plates were inoculated into 250 mL Erlenmeyer

flasks containing 50 mL GYMP broth (10 g/L glucose, 3 g/L yeast extract, 3 g/L malt extract, 2.5 g/L peptone). Flasks were incubated on an orbital shaker at 28 °C with 160 rpm agitation for 72 hours. Then, cultures were centrifuged (Sigma 3-30 K, Germany) at 10,000 × *g* for 10 min. Each 49.5 mL of culture supernatant was mixed with 0.5 mL of filter-sterilized AgNO₃ solution (200 mM). Subsequently, the mixture was incubated at 40 °C with 160 rpm agitation under dark conditions for three days and then subjected to centrifugation at 13,000 × *g* for 25 min. Mm-AgNPs were washed four times with 5 mL ultra-pure water (Millipore Milli-Q, USA) through centrifugation to remove medium components and unconverted silver ions. Finally, Mm-AgNPs were re-suspended in an equal volume of ultra-pure water. Obtained Mm-AgNPs stock solution was kept at 4 °C for further analysis. *Micromonospora* sp. SH121 culture supernatant without AgNO₃ and 2 mM AgNO₃ solution were used as controls.

Characterization of AgNPs

UV-Visible (UV-Vis) spectroscopy

A ten-fold dilution of the Mm-AgNPs stock solution was incubated in an ultrasonic bath (Daihan Scientific WUC-D06H, South Korea) for 5 min at 25 °C. The absorbance spectrum of the Mm-AgNPs in dilution was recorded using a microplate reader (Thermo Scientific Multiscan[®] Go, USA) in wavelengths ranging from 300 to 800 nm at a resolution of 1 nm. Culture supernatant without AgNO₃ and 2 mM AgNO₃ solution were used as controls.

Fourier transform infrared spectroscopy (FTIR)

Mm-AgNPs were freeze-dried and then subjected to FTIR analysis. FTIR analysis was carried out on PerkinElmer[®] Spectrum[™] 100 FT-IR spectrometer (Germany) in the range of 400–4000 cm⁻¹ wavelength with a resolution of 4 cm⁻¹.

Scanning electron microscopy (SEM)/energy dispersive X-ray spectroscopy (EDS)

A sufficient amount of Mm-AgNPs stock solution was dropped onto a 0.5 cm² glass slide and then dried at 25 °C for 24 h. Subsequently, samples were coated with a thin carbon layer and examined under a JEOL JSM-7001F field emission-scanning electron microscope (FESEM) operating at 15 kV. EDS mapping was carried out on the same slide using an X-Max 80 mm² detector (Oxford Instruments, UK) integrated to FESEM.

X-ray diffraction (XRD)

The crystal structure of the Mm-AgNPs was characterized by an XRD pattern drawn. The pattern was drawn with scanning of powdered Mm-AgNPs using Rigaku SmartLab (Rigaku Smartlab Beijing Co, Beijing, China) equipped with a Cu_K-beta filter in the range of 10–80° at 2 theta angle and a scanning rate of 2°/min. Scanning was carried out in the continuous mode at a voltage of 40 kV and a current of

30 mA. The crystallite size of Mm-AgNPs was estimated using Scherrer's equation.^[18]

Dynamic light scattering (DLS) and zeta potential

Mean diameter, size distribution, and surface charge of Mm-AgNPs in aqueous solution were measured using Malvern ZS zeta sizer at room temperature. AgNPs solution (1%) prepared with ultra-pure water was sonicated in the ultrasonic bath for 5 min before analysis.

Antimicrobial activity

Antimicrobial activity of Mm-AgNPs was evaluated against bacteria (*Acinetobacter baumannii* ATCC 19606, *Bacillus subtilis* ATCC 6051, *Bacillus cereus* RSKK 244, *Enterococcus faecalis* ATCC 29212, *Enterococcus hirae* ATCC 10541, *Escherichia coli* ATCC 25922, *Klebsiella pneumoniae* ATCC 10031, *Legionella pneumophila* ATCC 33152, *Proteus vulgaris* ATCC 33420, *Pseudomonas aeruginosa* ATCC 27853, *Pseudomonas putida* ATCC 47054, *Salmonella typhimurium* ATCC 14028, *Staphylococcus aureus* ATCC 25923, *Staphylococcus epidermidis* ATCC 12228, and *Streptococcus pneumoniae* ATCC 10015), filamentous fungi (*Aspergillus niger* ATCC 16404, *Aspergillus flavus* CCDCA 10508, *Fusarium oxysporum* MTCC-2480), and yeasts (*Candida albicans* ATCC 90028 and *Candida glabrata* ATCC 2001) by agar well diffusion and microdilution methods. Experiments were performed in triplicate.

Preparation of inoculum

Bacterial strains were incubated in MHB at 35 °C with 200 rpm agitation for 16 h. Bacteria were suspended in phosphate-buffered saline (PBS) after removing the medium by centrifugation at $10,000 \times g$ for 10 min. Bacterial cell concentration was calculated by the McFarland standard.^[19] Yeasts, incubated in YPDB at 28 °C with 200 rpm agitation for 24 h, were retrieved by centrifugation ($8,000 \times g$, 5 min). They were suspended in PBS and then counted by hemocytometer. Fungal spores were recovered by harvesting them from the YPDA with 1 mL of PBS containing 0.1% Tween 20, then counting with a hemocytometer. Finally, suspensions were diluted with PBS to obtain inoculum containing 3×10^7 cells or spores per milliliter.

Agar well diffusion method

First, 100 μ L inoculum was spread over the entire surface of the solid medium. The well with a diameter of 6 mm was punched in a solid medium by a cork-borer. The well was filled with 50 μ L of Mm-AgNPs colloidal suspension (100 μ g/mL). Distilled water was used as negative control.^[20] Bacterial strains were incubated at 35 °C for 24 h, while the fungal strains were grown at 28 °C for 72 h. Subsequently, diameter of inhibition zone (DIZ) around the well was measured. The method was applied using MHA and YPDA for bacterial and fungal strains, respectively.

Microdilution method

Minimum inhibitory concentration (MIC) and minimum bactericidal/fungicidal concentration (MBC/MFC) of Mm-AgNPs were detected on a 96-well microtiter plate by microdilution method.^[21] Wells were loaded with 290 μ L liquid medium containing different concentrations of Mm-AgNP and 10 μ L inoculum. MHB and YPDB were used as the liquid medium for bacteria and fungi, respectively. The final concentration of Mm-AgNPs in wells ranged from 0.5 to 512 μ g/mL. Microtiter plates containing bacterial cells were incubated at 35 °C for 24 h while the others were incubated at 28 °C for 48 h. The MIC was taken as the lowest concentration of Mm-AgNPs, inhibiting the visible microbial growth. Cultures (50 μ L) in wells where microbial growth is not detected were spread on the solid medium, followed by incubation for 48 h. Microbial growth was checked at the end of incubation at 35 °C and 28 °C for bacteria and fungi, respectively. The MBC and MFC were defined as the minimum concentration of Mm-AgNPs that killed bacteria and fungi, respectively.

Antibiofilm activity

The crystal violet biofilm formation assay with a slight modification was used to assess the antibiofilm activity of Mm-AgNPs.^[22,23] As mentioned in the microdilution method, the experiment was designed on 96-well flat-bottom microtiter plates. Microorganisms with biofilm formation ability (*A. baumannii*, *E. coli*, *E. faecalis*, *K. pneumoniae*, *P. aeruginosa*, *S. aureus*, *C. albicans*, and *C. glabrata*) were incubated for 72 h under static condition. Each microorganism was exposed to nanoparticles at 1/4, 2/4, and 3/4 of the Mm-AgNPs concentration corresponding to its MIC value during incubation. At the end of incubation, wells were washed with distilled water three times. Subsequently, 200 μ L of 0.5% crystal violet solution was transferred to each well to stain the remaining microorganisms. The excess dye was removed by washing with distilled water. Dye adsorbed by microorganisms was solubilized using 200 μ L of 95% ethanol. Finally, the absorbances of solutions were measured at 570 nm to assess adherent microorganism density.

DNA cleavage activity

DNA cleavage activity of Mm-AgNPs was assessed using pBluescript SK II phagemid DNA extracted from chemically competent *E. coli* TOP10 cells. The mixture, containing 2 μ L of phagemid DNA and 2 μ L of Mm-AgNPs suspension (8–1024 μ g/mL), incubated at 37 °C for 2 h. Subsequently, 4 μ g of loading buffer was added to the mixture. Different forms of phagemid DNA were separated using 1% agarose gel at 100 V using a horizontal electrophoresis system (Cleaver Scientific, Warwickshire, UK). Finally, forms of DNA were visualized using ChemiDOC MP Imaging System (Bio-Rad Laboratories, Hercules, CA, USA).

Anticancer activity of Mm-AgNPs

Cell culture

The human prostate carcinoma cell line DU145 was used to evaluate the anticancer activity of Mm-AgNPs. Additionally, healthy human dermal fibroblast cells were used for comparison. DU145 and dermal fibroblast cells were grown in RPMI-1640 with the addition of 10% fetal bovine serum, 100 U/mL of penicillin, and 100 mg/mL of streptomycin. The cells were incubated in an incubator at 37°C in 5% CO₂. The culture medium was changed every 3–4 days.

In vitro cytotoxicity assay

In vitro cytotoxicity of Mm-AgNPs was determined using the xCELLigence Real-Time Cell Analysis DP instrument (Roche Diagnostics GmbH, Penzberg). DU145 and dermal fibroblast cells were passaged after 90% confluency. After seeding 200 µL of the cell suspensions in RPMI-1640 containing 10% FBS into the wells (10,000 cells/well) of the E-plate 16. Cells were allowed to adhere to the E-plate for 24 h. Then, the media was removed from the well. Cells were treated with different doses of Mm-AgNPs (1, 10, 100, 500, and 1000 µg/mL). The proliferation in the DU145 cells were monitored every 15 min for 92 h by the xCELLigence device. Cell proliferation experiments were performed in triplicate. The complete growth medium was used as control for cytotoxicity assay.

Comet assay

After reaching confluence, the DU145 cells were harvested, and 15×10^4 cells/well were plated in 24 well tissue culture plates. After being allowed to be attached for 24 h, the cells were exposed to increasing concentrations of Mm-AgNPs (1, 10, and 100 µg/mL) to evaluate genotoxicity for 24 h. Also, hydrogen peroxide was used as a positive control for the genotoxicity assay. When exposure expired, cells were washed with PBS and subjected to the alkaline comet assay to evaluate the DNA strand breaks.

Alkaline comet assay was applied as described by Singh et al.^[24] Briefly, microscope slides were covered with standard melting point agarose. Then, 10^4 cells were suspended in 100 µL low melting point agarose. After then, the mixture was shed onto pre-coated microscope slides. The slides were covered with a coverslip for 20 minutes at 4°C. The coverslip was removed, and the slides were submerged into freshly cold lysis buffer for 1 hour in the dark. Then, the slides were electrophoresed for 30 minutes using a voltage of 24 V and a current of 300 mA. Following electrophoresis, slides were transferred to a neutralization solution. The slides were stained with ethidium bromide and were evaluated using a fluorescence microscope for DNA damage as tail length. The complete growth medium and hydrogen peroxide were used as controls in the comet assay.

Apoptosis detection in DU145 cells by annexin V/propidium iodide assay

The Annexin V/Propidium iodide staining technique followed by flow cytometry was performed to assess the cell death induced in DU145 cells by Mm-AgNPs. The cells were treated with Mm-AgNPs (1, 10, and 100 µg/mL) for 24 h. After incubation, the cells were collected and stained according to the manufacturer's recommendations (BioLegend's APC Annexin V Apoptosis Detection Kit with Propidium iodide (PI) (cat. No. 640932 Biolegend, San Diego, CA). The percentages of apoptosis were measured on the BD FACSAria™ III flow cytometer (BD Biosciences, Bedford, MA, USA) using FACS Diva Software.

Results and discussion

Synthesis of Mm-AgNPs

The culture supernatant of pigment-producing *Micromonospora* sp. SH121 (Supplementary Materials 1 and 2) was used as a source of reducing and capping agents for Mm-AgNPs synthesis. The synthesis, initiated by adding AgNO₃ solution to the culture supernatant, was carried out by incubating the mixture at 40°C with 160 rpm shaking for 3 days. The reduction of AgNO₃ into Mm-AgNPs was visually confirmed by color change from pale yellow (Figure 1a) to dark brown (Figure 1b). On the other hand, the colors of AgNO₃ solution (2 mM) and culture supernatant without AgNO₃ did not change under the same conditions.

Characterization of Mm-AgNPs

UV-Vis spectrum of Mm-AgNPs

UV-Vis spectral analysis was carried out to confirm AgNPs synthesis and pre-assessment of synthesized AgNPs. According to the literature, the oscillation of electrons on the surface of the nanoparticles causes an obvious surface

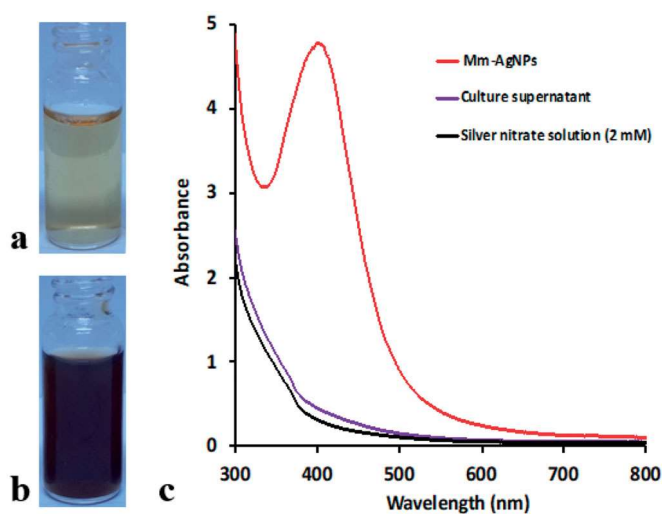


Figure 1. Mm-AgNPs triggered color change from pale yellow (a) and dark brown (b) in the reaction mixture. The UV-Vis spectra of Mm-AgNPs (red line), *Micromonospora* sp. SH121 culture supernatant (purple line) and 2 mM silver nitrate solution (black line) (c).

plasmon resonance (SPR) peak between 400–500 nm of the spectrum, as shown in Figure 1c.^[2] Further, there is a relationship between SPR peak position and nanoparticle size.^[25] The SPR peak position shifts from the violet region (400–420 nm) of the spectrum to the blue region (440–490 nm) as the size of the silver nanoparticles increases. On the other hand, sharp SPR peaks indicate that particle sizes are distributed within narrow ranges. In the present study, Mm-AgNPs had shown the typical SPR peak at 402 nm (λ_{max}). Such SPR peak was not observed in control. This result revealed that the Mm-AgNPs exhibited unique optic properties from the counterparts synthesized by microorganisms.^[26–28]

FTIR spectrum of Mm-AgNPs

FTIR study was conducted to identify the functional groups on Mm-AgNPs and estimate bio-active molecules responsible for their formation and stabilization. FTIR spectrum of Mm-AgNPs is shown in Figure 2. The broadband seen at 3331.7 cm^{-1} corresponds to the carbonyl stretch of the hydroxyl group in phenols such as 2,5-bis(1,1-dimethyl ethyl) phenol, benzene acetic acid, and 1,1-diphenyl-2-picrylhydrazyl, which were secreted by the strain.^[29,30] Bands shown at 2959.2 and 2859.2 are the characteristic of C–H stretching in the alkanes. The band at 1724 cm^{-1} corresponds to C=O stretching. A sharp peak at 1637.9 cm^{-1} , which arose from the C=O stretching vibration and is known as the Amide I band, is characteristic of proteins. The position of the Amide I band implies that the major secondary structure of proteins on the surface of nanoparticles is antiparallel β -sheets. It also means that the conformational specificity of the proteins is largely conserved. The band at 1268.6 corresponds to the stretching vibration of the C–N group (Amide III) in proteins. On the other hand, bands at 1460.7 and 729.4 cm^{-1} are due to the bending vibration of C–H and C=C groups in glycolipids, respectively. Bands at 1117.2 and 1019.3 are a result of C–O stretching vibration. To sum up, FTIR analysis

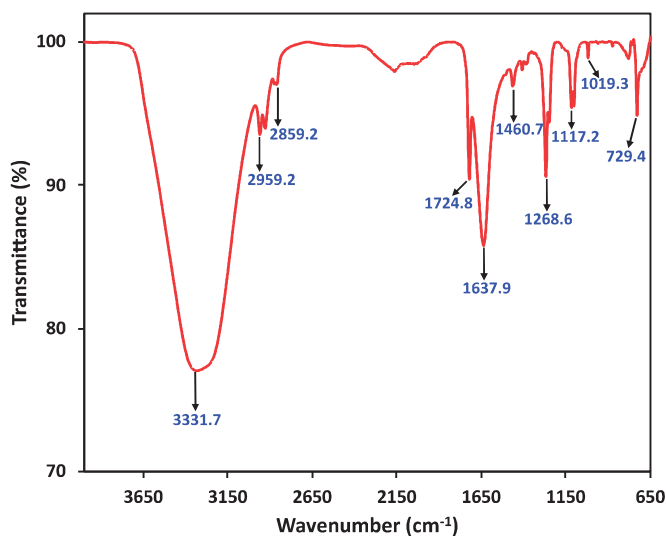


Figure 2. FTIR spectrum of Mm-AgNPs.

showed that phenols, proteins, and biosurfactants play a significant role in forming and stabilizing Mm-AgNPs.

The mechanism of AgNPs synthesis by bacterial culture supernatant consist of three stages; (i) reduction (ii) growth, and (iii) capping and stabilization.^[31] The proposed mechanism was schematized in supplementary material 4. It is suggested that several hypotheses for the reduction which is the most critical stage. Many researchers have stated that ADH-dependent enzymes secreted from bacteria may be responsible for reducing Ag ions to elemental silver. On the other hand, some others have claimed that silver-specific proteins, spore-associated enzymes, and various peptides play an essential role in reducing silver ions.^[32] Similar to our study, there is no study in the literature describing the specific biomolecules involved in AgNPs synthesis in detail.

SEM-EDS analysis of Mm-AgNPs

Electron micrographs were taken at magnifications of 25,000 (Figure 3a) and 100,000 (Figure 3b) to assess the morphological structure of Mm-AgNPs. Micrographs clearly show that Mm-AgNPs were almost spherical. Mm-AgNPs were in the range of 10–30 nm, as predicted by the UV-Vis spectral analysis. On the other hand, most of the particles were clustered into agglomerates smaller than 50 nm in diameter. The aggregation may be related to functional groups detected by FTIR analysis (Figure 2) on the surface of Mm-AgNPs.

EDS analysis was performed to determine the elemental composition of the FESEM sample. In the EDS spectrum displayed in Figure 4, the strongest signal was obtained for silver atoms. Moderate signals were also observed for the Si and C elements due to the carbon-coated borosilicate glass used in sample preparation. On the other hand, weak signals for oxygen, nitrogen, calcium, magnesium, and sodium were detected in the spectrum, thought to be caused by biomolecules bound to the surface of the reduced Ag ions.

XRD pattern of Mm-AgNPs

The XRD pattern of Mm-AgNPs is shown in Figure 5. Four intense peaks at 38.05° , 46.27° , 64.72° , and 77.5° specified to (111), (200), (220), and (311) planes, respectively. Apart from the pattern, it was deduced that the crystalline nature of Mm-AgNPs displayed “face centered cubic (fcc)” structure. Similar results have been reported for AgNPs synthesized by other actinobacterial strains including *Streptomyces violaceus*,^[33] *Streptomyces* sp. EMB24,^[34] *Rhodococcus rhodochrous*,^[35] *Streptomyces olivaceus*,^[36] *Nocardioopsis dassonvillei*,^[37] *Pilimelia columellifera* SF23,^[38] and *Streptomyces* sp. OSIP1.^[39] The data has been observed to match the The Joint Committee on Powder Diffraction Standards (JCPDS) file with 89-3722 reference number. A weak peak located at a 2-theta degree of 32.27 revealed the presence of organic substances at the surface of Mm-AgNPs.^[40] Furthermore, the crystallite size of Mm-AgNPs were calculated from XRD data using Debye–Scherrer equation is given below:

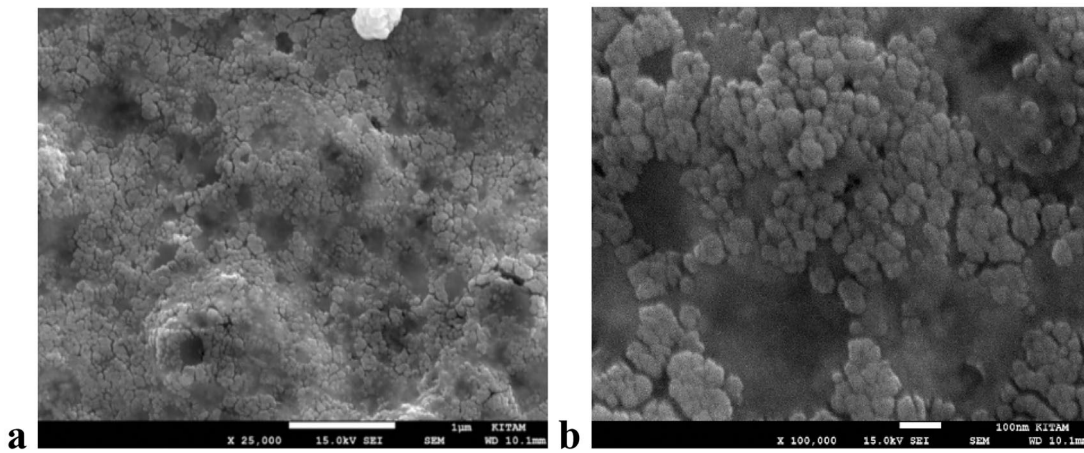


Figure 3. FESEM Micrograph of Mm-AgNPs in 25,000 \times (a) and 100,000 \times (b) magnification with 15.0 Kv.

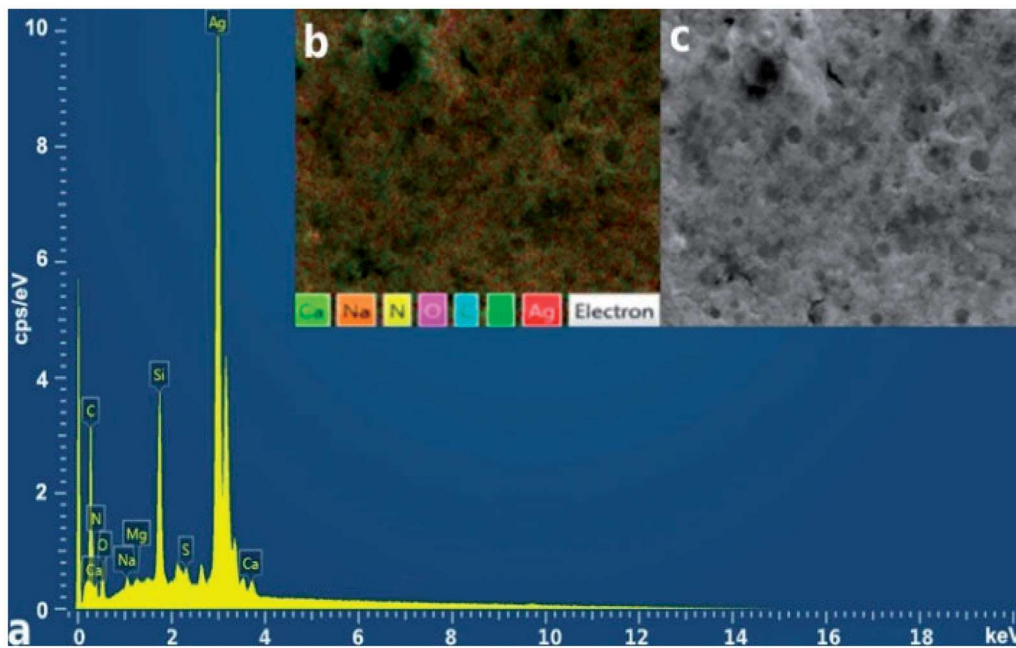


Figure 4. The EDS spectrum (a) and elemental mapping image (b) of Mm-AgNPs sample (c).

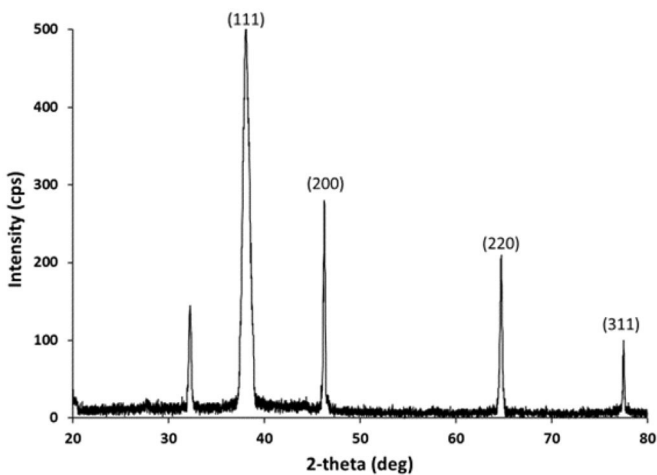


Figure 5. XRD pattern of powdered Mm-AgNPs.

$$\text{Crystallite size} = \frac{K\lambda}{\beta \cos \theta} \quad (1)$$

where K , λ , β , and θ are Scherrer constant (0.9), X-ray wavelength (0.15406 nm), full line width at half maximum (FWHM), and Bragg diffraction angle, respectively. The mean crystallite size of Mm-AgNPs, calculated as 13 nm, was smaller than that of AgNPs synthesized by *Streptomyces* sp. MOSEL-ME28,^[35] *Streptomyces antimycoticus* L-1,^[26] and *Streptacidiphilus* sp. strain CGG11.^[41]

DLS and zeta potential analyses of Mm-AgNPs

Particle size distribution is a crucial factor for the use of nanoparticles in industrial and clinical applications. A successful formulation requires the monodisperse preparation of silver nanoparticles. DLS analysis was performed at 25°C

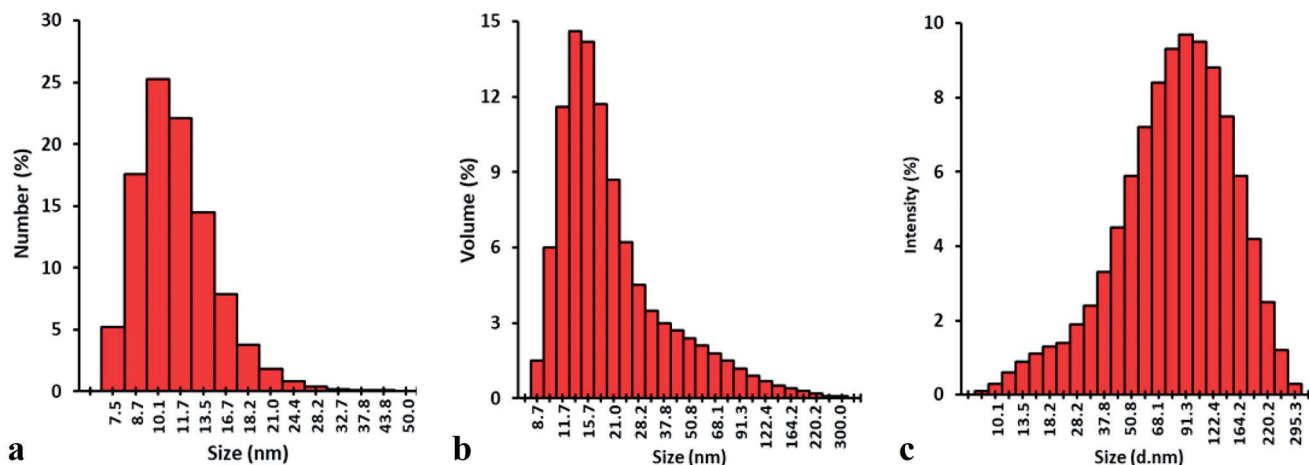


Figure 6. Particle size distribution of Mm AgNPs on the basis of number (a), volume (b), and intensity (c).

in pure water with a dispersant refractive index of 1.33 and a viscosity of 0.8872 to detect the polydispersity index (PDI) value, reflecting the size distribution of Mm-AgNPs. A colloidal nanoparticle solution with a PDI value less than 0.3 is considered monodisperse. Z-average hydrodynamic diameter and PDI value of Mm-AgNPs were found to be 65.57 and 0.284, respectively. Results indicated that the Mm-AgNPs have a more homogenous distribution than many AgNPs synthesized by bacteria.^[42,43] Further, the Z-average hydrodynamic diameter was smaller than their bacteria-mediated counterparts.^[44] The particle size distribution of Mm AgNPs based on number, volume, and intensity is shown in **Figure 6**.

Another critical factor in the use of nanoparticles in biotechnological applications is their stability in colloidal suspensions. In general, zeta potential less than -30 mV or higher than $+30$ mV indicates that nanoparticles are stable and well dispersed due to electrostatic repulsion. On the other hand, AgNPs with a zeta potential close to neutral values tend to coagulate and agglomerate. Mm-AgNPs exhibited high negative polarity with a zeta potential of -35.3 mV due to capping agents surrounding the surface of reduced silver ions (**Figure 7a**). In many studies, it has been reported that the zeta potential values for AgNPs synthesized using Actinobacteria were range of -30 mV to -15 mV.^[45-47] Result also revealed that the Mm-AgNPs was noteworthy stable. To test the finding, Mm-AgNPs suspensions (1 mg/mL) were kept at room temperature for 90, 180, 270, and 360 days. Afterward, absorbance spectrums of suspensions were checked by UV-vis spectroscopy. Results showed that the SPR peak intensity of Mm-AgNPs decreased in a time-dependent manner (**Figure 7b**). However, the SPR peak position did not alter after incubating for 270 days.

Antimicrobial activity

Based on the diameter of inhibition zones given in **Table 1**, it was seen that the Mm-AgNPs exhibit an excellent antimicrobial effect. AgNPs formed wider inhibition zones compared to the positive controls for both bacteria and fungi. It was also noted that the Mm-AgNPs were more effective

against fungi than bacteria. The lower sensitivity of fungi may be due to the differences in the cell wall structure and cellular organization. The most sensitive bacterial strain was *E. coli* with an inhibition zone of 25.1 ± 1.0 mm. Mm-AgNPs also exhibited a high antibacterial effect against *P. vulgaris*, *K. pneumoniae*, *E. faecalis*, *B. cereus*, *E. hirae*, *S. epidermidis*, with inhibition zones of 24.0 ± 0.5 , 22.1 ± 0.1 , 20.8 ± 0.8 , 20.4 ± 0.5 , 20.3 ± 0.6 , 20.0 ± 0.6 and 19.0 ± 1.0 , respectively. The most resistant bacterial strain was *L. pneumophila*, with an inhibition zone of 16.7 ± 0.6 . Concerning fungi, the highest effect was recorded against *C. albicans* (16.9 ± 0.4 mm), followed by *A. flavus* (15.7 ± 0.5 mm), *A. niger* (14.5 ± 0.2 mm), and *C. glabrata* (14.3 ± 0.7 mm). The sizes of inhibition zones were 12.8 ± 0.1 and 11.1 ± 0.4 for *F. oxysporum* and *R. stolonifera*, respectively. The negative control showed no zone of inhibition against bacteria and fungi.

MIC and MBC/MFC values of Mm-AgNPs against tested strains were consistent with the agar well diffusion method results (**Table 2**). The Mm-AgNPs exhibited a higher inhibitory effect with a MIC value of $4 \mu\text{g/mL}$ against *E. coli*, *P. vulgaris*, *S. typhimurium* and *S. epidermidis* among the bacterial strains. In addition, a relatively low MIC value ($8-32 \mu\text{g/mL}$) was recorded for other bacterial strains, except for *L. pneumophila* ($256 \mu\text{g/mL}$). MBC values lower than $64 \mu\text{g/mL}$ are considered strong antimicrobial action. The highest bactericidal effect was expressed against *E. coli* and *P. vulgaris*, which were the most sensitive to the Mm-AgNPs with an MBC value of $8 \mu\text{g/mL}$, followed by *E. faecalis*, *E. hirae*, *P. putida*, and *S. epidermidis* with $8 \mu\text{g/mL}$ an MBC value of $16 \mu\text{g/mL}$. On the other hand, it was noted that the Mm-AgNPs did not show a significant bactericidal effect against *P. aeruginosa* and *L. pneumophila*. *A. flavus* was the most susceptible fungi to Mm-AgNPs with MIC and MFC values of 8 and $32 \mu\text{g/mL}$, respectively. The inhibitory effect of Mm-AgNPs against other tested fungi was also strong with MIC values of $\leq 64 \mu\text{g/mL}$, whereas their fungicidal effect was moderate with MFC values ranging from 64 to $256 \mu\text{g/mL}$. According to the results, Mm-AgNPs exhibit a strong antimicrobial effect more than many other counterparts reported previously. Aygün et al.^[48] reported that MIC values of green synthesized AgNPs against *E. coli*, *E. hirae*,

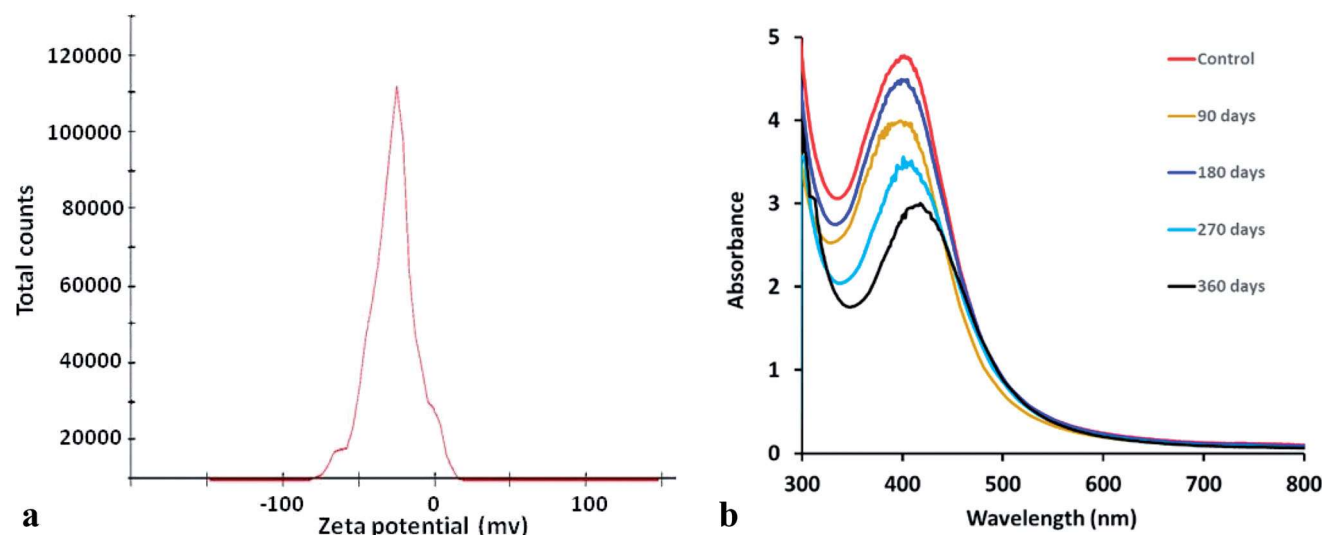


Figure 7. Zeta potential (a) and UV-Vis spectrum of Mm-AgNPs suspension kept at room temperature for different times (0–360 days) (b).

Table 1. Diameter of inhibition zone caused by the antimicrobial activity of Mm-AgNPs, streptomycin sulfate, and nystatin.

Microorganisms	Diameter of inhibition zone (mm)		
	Mm-AgNPs	Streptomycin sulfate	Nystatin
Bacteria			
<i>A. baumannii</i>	18.2 ± 0.3	–	–
<i>B. subtilis</i>	19.7 ± 0.6	18.4 ± 0.5	–
<i>B. cereus</i>	20.4 ± 0.5	18.7 ± 0.2	–
<i>E. faecalis</i>	20.8 ± 0.8	20.0 ± 0.5	–
<i>E. hirae</i>	20.3 ± 0.6	17.5 ± 0.3	–
<i>E. coli</i>	25.0 ± 1.0	16.4 ± 0.7	–
<i>K. pneumoniae</i>	22.1 ± 0.1	24.0 ± 0.4	–
<i>L. pneumophila</i>	16.7 ± 0.6	15.2 ± 0.3	–
<i>P. vulgaris</i>	24.0 ± 0.5	22.3 ± 0.6	–
<i>P. aeruginosa</i>	17.5 ± 0.5	6.2 ± 0.5	–
<i>P. putida</i>	17.1 ± 0.3	9.5 ± 0.8	–
<i>S. typhimurium</i>	17.8 ± 0.6	–	–
<i>S. aureus</i>	19.0 ± 1.0	18.2 ± 0.3	–
<i>S. epidermidis</i>	20.0 ± 0.6	18.5 ± 1.0	–
<i>S. pneumoniae</i>	17.3 ± 0.2	17.4 ± 0.7	–
Fungi			
Yeasts			
<i>C. albicans</i>	16.9 ± 0.4	–	9.9 ± 0.5
<i>C. glabrata</i>	14.3 ± 0.7	–	9.0 ± 0.3
Filamentous fungi			
<i>A. niger</i>	14.5 ± 0.2	–	3.2 ± 0.3
<i>A. flavus</i>	15.7 ± 0.5	–	3.6 ± 0.2
<i>F. oxysporum</i>	12.8 ± 0.1	–	5.5 ± 0.1
<i>R. stolonifer</i>	11.1 ± 0.4	–	6.8 ± 0.4

S. aureus, *P. aeruginosa*, *B. cereus*, and *C. albicans* were 16, 128, 64, 32, 128, and 512 µg/mL, respectively. Ulagesan et al.^[49] detected that the MIC and MBC values of AgNPs synthesized using *Pyropia yezoensis* were 200 and 400 µg/mL, against *P. aeruginosa*, respectively.^[50] It has been reported that AgNPs synthesized by *Rothia endophytica* showed inhibitory and fungicidal effect against *C. albicans* at concentrations of 65.5 and 125 µg/mL, respectively.^[51] Anasane et al.^[46] studied the antifungal activity of AgNPs synthesized by *P. columellifera* C9, an acidophilic actinobacterium. Their MIC value against *C. albicans* was 40 µg/mL. In another study, MIC values of AgNPs synthesized using *Allium ampeloprasum* aqueous extract ranged from 17.25 to 35 µg/mL against *E. coli*, *P. aeruginosa* and *S. aureus*.^[52]

Table 2. MIC and MBC/MFC values of Mm-AgNPs against microorganisms.

Microorganisms	MIC	MBC/MFC
Bacteria		
<i>A. baumannii</i>	16	64
<i>B. subtilis</i>	16	32
<i>B. cereus</i>	8	32
<i>E. faecalis</i>	8	16
<i>E. hirae</i>	8	16
<i>E. coli</i>	4	8
<i>K. pneumoniae</i>	8	32
<i>L. pneumophila</i>	256	–
<i>P. vulgaris</i>	4	8
<i>P. aeruginosa</i>	32	256
<i>P. putida</i>	8	16
<i>S. typhimurium</i>	4	64
<i>S. aureus</i>	16	64
<i>S. epidermidis</i>	4	16
<i>S. pneumoniae</i>	16	32
Fungi		
Yeasts		
<i>C. albicans</i>	32	64
<i>C. glabrata</i>	32	128
Filamentous fungi		
<i>A. flavus</i>	8	32
<i>A. niger</i>	16	256
<i>F. oxysporum</i>	64	256
<i>R. stolonifer</i>	32	256

– Not detected.

Results also depicted those various factors such as morphology, stability, and surface charge play a critical role on the antimicrobial efficiency of AgNPs.^[53] A possible reason for the broad-spectrum effect of AgNPs is that they form irreversible S-Ag bonds with thiol groups in enzymes located on the cell membrane, thereby inactivating energy generation, increasing the membrane permeability, and triggering ROS production, causing eventual cell death.^[54]

In addition, Mm-AgNPs exhibited excellent antimicrobial effects under non-sterile conditions (Supplementary material 3). Consequently, the broad-spectrum antimicrobial property of Mm-AgNPs makes them a preferable additive in hygiene products, cosmetics, food packages,^[55] punches, and medical clothes and devices.

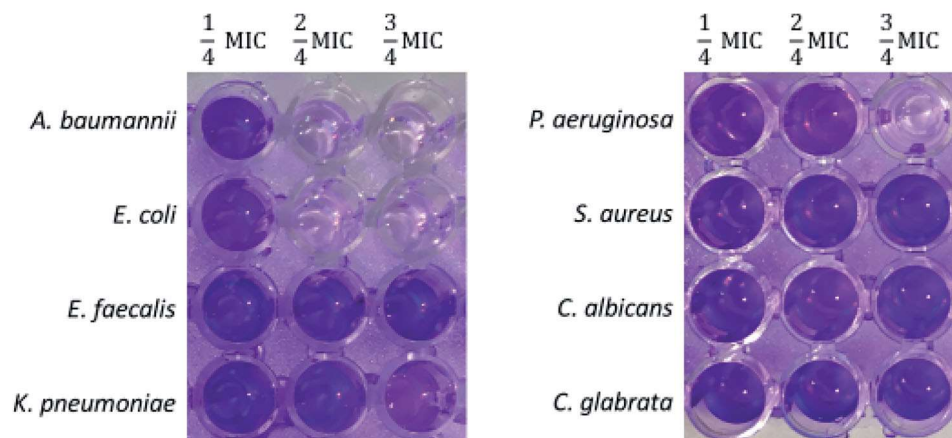


Figure 8. Wells with and without biofilm formation after crystal violet biofilm formation assay.

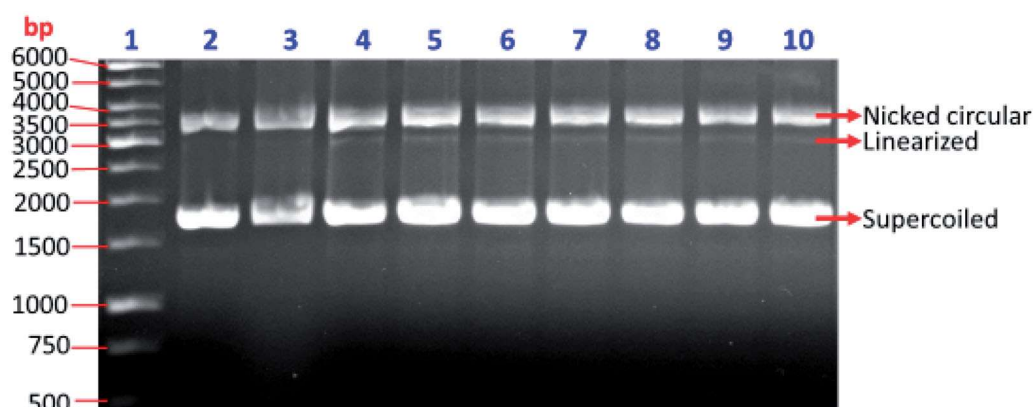


Figure 9. Cleavage of pBluescript SK II phagemid DNA by Mm-AgNPs. Sizes of phagemid DNA forms were estimated using a DNA ladder (Line 1). Phagemid DNA incubated without Mm-AgNPs was used as a control (Line 2). Phagemid DNAs separately incubated with 4, 8, 16, 32, 64, 128, 256, and 516 $\mu\text{g/mL}$ Mm-AgNPs were shown in Line 3, Line 4, Line 5, Line 6, Line 7, Line 8, Line 9, and Line 10, respectively.

Antibiofilm activity

Results indicated that the 2, 8, and 28 $\mu\text{g/mL}$ of Mm-AgNPs inhibited biofilm formation in *E. coli*, *A. baumannii*, and *P. aeruginosa*, respectively (Figure 8). The biofilm formation ability of *K. pneumoniae* was considerably decreased by incubation with 6 $\mu\text{g/mL}$ Mm-AgNPs. On the other hand, antibiofilm activity of Mm-AgNPs against *E. faecalis*, *S. aureus*, *C. albicans*, and *C. glabrata* was pretty weak. It was clearly seen that Mm-AgNPs exhibited better antibiofilm activity against Gram-negative bacterial strains. It may be due to the presence of a lipopolysaccharide layer surrounding peptidoglycan in the cell wall of Gram-negative bacteria, unlike Gram-positive bacteria. Similar findings have been reported for biosynthesized AgNPs.^[56–59] Zamanpour et al.^[60] stated that the presence of 62 $\mu\text{g/mL}$ AgNPs synthesized by *Vibrio* sp. B4L completely hindered the biofilm formation ability. Singh et al.^[61] depicted that biofilm formation significantly diminished when the *E. coli* and *S. aureus* were incubated with *Cedecea* sp. mediated biosynthesized AgNPs at a concentration of 12.5 and 100 $\mu\text{g/mL}$, respectively. It has been reported that the antibiofilm activity of AgNPs could be

related to cell growth inhibition, cell structure deterioration, and biofilm layer destruction.^[62]

DNA cleavage activity

DNA cleavage activity of Mm-AgNPs was evaluated by monitoring supercoiled, nicked, and linearized forms of pBluescript SK II phagemid DNA. DNA forms separated in agarose gel (Figure 9) were quantified using Image J software. From the results, no significant change was detected in the intensity of supercoiled DNA after the phagemid was incubated with different concentrations of Mm-AgNPs. The intensity of the band, which corresponds to the linearized form of phagemid DNA, increased when Mm-AgNPs concentration was up to 16 $\mu\text{g/mL}$. On the other hand, a further increase in Mm-AgNPs did not cause an alteration in the band intensity. Briefly, the DNA cleavage activity of Mm-AgNPs was not statistically significant. Unlike our findings, some previous studies demonstrated that AgNPs cause breaks in plasmid DNA.^[63–65] In such studies, it has been claimed that the main reason for the antimicrobial effect of AgNPs may be their DNA cleavage activity.^[48]

Anticancer activity of Mm-AgNPs on prostate cancer cell line

Monitoring of cytotoxicity of Mm-AgNPs on DU 145 prostate cancer cells using xCELLigence system

Cytotoxic effect of Mm-AgNPs in the range 1 $\mu\text{g}/\text{mL}$ – 1 mg/mL to DU 145 and human dermal fibroblast cells was determined using the xCELLigence system. The cell proliferation index values of DU 145 and human dermal fibroblast cells after exposure to Mm-AgNPs for 24, 48, and 72 h are shown in [Supplementary Material 5](#). As expected, a dose-dependent decrease in cell index value was observed for

Table 3. The proportion of type 0 (T 0), type I (T I), type II (T II), type III (T III), and type IV (T IV) cell types in every 100 cells, the percentage of damaged cells (DC), and genetic damage index (GDI).

Groups	T 0	T I	T II	T III	T IV	DC (%)	GDI
Negative control	61.0	14.5	11.5	5.5	7.5	24.5 \pm 9.9	0.8 \pm 0.2
Positive control	46.0	12.0	13.0	13.3	15.8	42.0 \pm 4.6	1.4 \pm 0.1
1 $\mu\text{g}/\text{mL}$ Mm-AgNPs	39.0	19.0	15.0	11.0	16.0	42.0 \pm 9.2	1.5 \pm 0.2
10 $\mu\text{g}/\text{mL}$ Mm-AgNPs	36.0	11.0	13.5	13.0	26.5	53.0 \pm 7.4	1.8 \pm 0.2
100 $\mu\text{g}/\text{mL}$ Mm-AgNPs	11.5	14.5	15.5	17.5	41.0	74.0 \pm 6.7	2.6 \pm 0.3

Table 4. Evaluation of apoptosis/necrosis in DU 145 cells treated with Mm-AgNPs for 24 hours using the Annexin-V-PI assay in flow cytometry.

Groups	Live cells	Early apoptosis	Late apoptosis	Necrosis
Control	82.20 \pm 4.84	1.16 \pm 2.02	2.56 \pm 3.75	12.66 \pm 0.92
1 $\mu\text{g}/\text{mL}$ Mm-AgNPs	68.37 \pm 0.90	9.20 \pm 0.60	12.10 \pm 1.15	10.36 \pm 0.83
10 $\mu\text{g}/\text{mL}$ Mm-AgNPs	67.80 \pm 4.94	7.73 \pm 3.39	11.60 \pm 2.28	12.83 \pm 1.92
100 $\mu\text{g}/\text{mL}$ Mm-AgNPs	71.23 \pm 4.11	5.36 \pm 4.89	7.16 \pm 5.53	16.26 \pm 6.43

fibroblast cells. In contrast, surprisingly, the cell index value was lower than the other doses when DU145 cells were exposed to the 1 $\mu\text{g}/\text{mL}$ concentration of Mm-AgNPs. Moreover, it was observed that Mm-AgNPs exhibited a more cytotoxic effect on DU 145 cells than fibroblast cells at 1 $\mu\text{g}/\text{mL}$ concentration.

Comet assay

The alkaline comet assay was used to evaluate the DNA damage at the experimental series of Mm-AgNPs treatments. The DNA damage was measured as the mean comet tail length. According to the tail length, the cells were classified into five types. These were type 0, type I, type II, type III, and Type IV. The proportion of intact and damaged cell types in every 100 cells is shown in [Table 3](#). It was found to be a significant increase in the DNA damage at the rising dose of Mm-AgNPs. Following Mm-AgNPs exposure, a rise of the damaged cells % in DU 145 cells was detected. Moreover, it was determined a significant increase in GDI with Mm-AgNPs exposure compared to the negative control. The highest genetic damage index was observed as 2.6 at the 100 $\mu\text{g}/\text{mL}$ Mm-AgNPs group for 24 hours. The lowest genetic damage index was 0.8 at the negative control group. Consequently, it was determined genotoxic of rising Mm-AgNPs doses in the DU 145 cells for 24 h.

Apoptosis

Following 24 h of treatment of DU 145 cells with different Mm-AgNPs doses, flow cytometry was used to determine

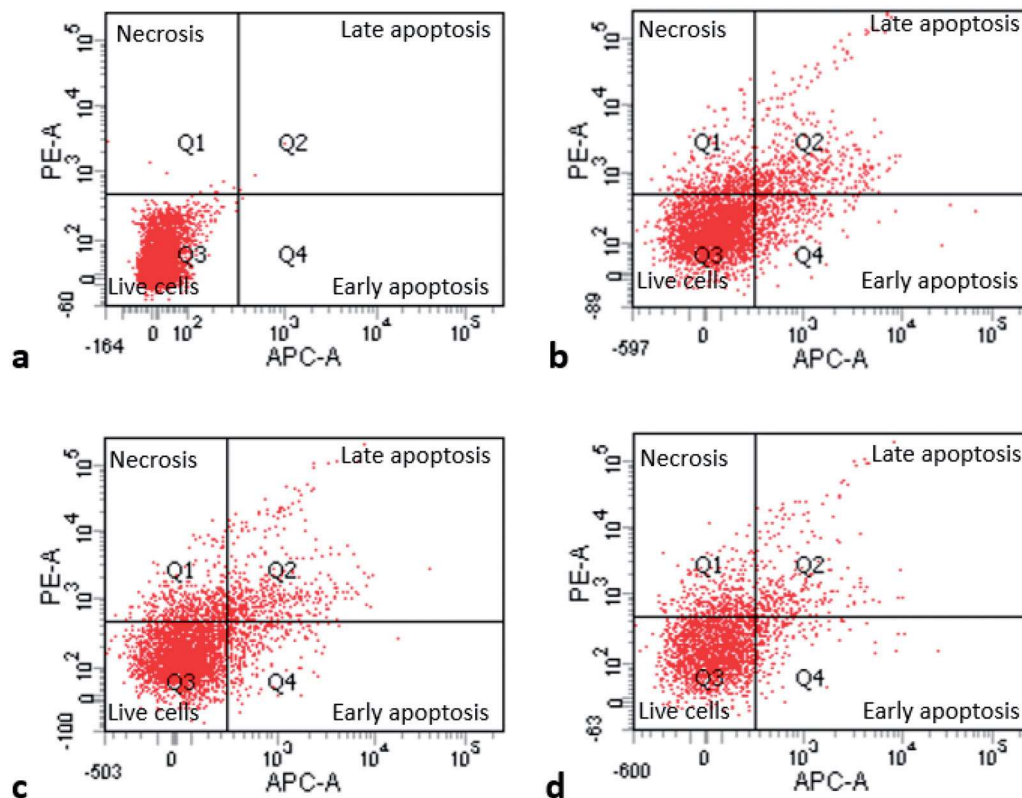


Figure 10. Dot plots from flow cytometry analysis performed with Annexin-V/PI staining are shown in untreated DU 145 cells (a), DU 145 cells treated with 1 $\mu\text{g}/\text{mL}$ Mm-AgNPs for 24 h (b), DU 145 cells treated with 10 $\mu\text{g}/\text{mL}$ Mm-AgNPs for 24 h (c), and DU 145 cells treated with 100 $\mu\text{g}/\text{mL}$ Mm-AgNPs for 24 h (d).

apoptosis and necrosis. When the parameters were measured, 1 µg/mL Mm-AgNPs treated induced higher levels of apoptosis in DU 145 cells than in other groups (Table 4 and Figure 10). However, it was observed that the necrosis increased in the treated group with 100 µg/mL AgNPs. The data of other Mm-AgNPs groups was similar to the control.

The normal human dermal fibroblasts cells were used as a control to determine the cytotoxic and apoptotic effect of Mm-AgNPs. It was observed that the cell index value started to decrease at doses of 100 µg and above. Therefore, the 100 µg Mm-AgNPs dose was used to determine the apoptotic effect in normal cells. The apoptosis and necrosis values were obtained similar to the negative control value. According to our data, the effect mechanism of Mm-AgNPs on normal and cancer cells was different. While the low doses (1 and 10 µg/mL Mm-AgNPs) did not show apoptotic and cytotoxic effects in normal cells, it was observed that it caused cytotoxic, genotoxic, and apoptotic effects in cancer cells.

Conclusion

In this study, we applied the green chemistry approach, which used culture supernatant of pigment-producing *Micromonospora* sp. SH121 to synthesize AgNPs. Mm-AgNPs with polydispersity index of 0.284 and zeta potential value of -35.3 mV were highly stable, which provides them with excellent interaction potential with cells or substances. Functional groups detected on Mm-AgNPs by FTIR analysis facilitate binding to surfaces and drugs. Mm-AgNPs showed encouraging properties for pharmaceutical industries due to broad-spectrum antimicrobial activity. Furthermore, results revealed that Mm-AgNPs might be a potential therapeutic for prostate cancer treatment in the future.

Disclosure statement

No potential conflict of interest was reported to the author(s).

Funding

This study was supported by the Research Fund of Mersin University with project number 2019-1-AP4-3355.

References

- [1] Kobeissi, E.; Menassa, M.; Moussally, K.; Repetto, E.; Soboh, I.; Hajjar, M.; Saleh, S.; Abu-Sittah, G. The Socioeconomic Burden of Antibiotic Resistance in Conflict-Affected Settings and Refugee Hosting Countries: A Systematic Scoping Review. *Confl. Health.* **2021**, *15*, 21–29.
- [2] Prema, P.; Veeramanikandan, V.; Rameshkumar, K.; Gatasheh, M. K.; Hatamleh, A. A.; Balasubramani, R.; Balaji, P. Statistical Optimization of Silver Nanoparticle Synthesis by Green Tea Extract and Its Efficacy on Colorimetric Detection of Mercury from Industrial Waste Water. *Environ. Res.* **2022**, *204*, 111915.
- [3] US Pharmacopeia. Antimicrobial Resistance. <https://www.usp.org/our-impact/antimicrobial-resistance> (Accessed May 10, 2022).
- [4] Gómez-Núñez, M. F.; Castillo-López, M.; Sevilla-Castillo, F.; Roque-Reyes, O. J.; Romero-Lechuga, F.; Medina-Santos, D. I.; Martínez-Daniel, R.; Peón, A. N. Nanoparticle-Based Devices in the Control of Antibiotic Resistant Bacteria. *Front. Microbiol.* **2020**, *11*, 563821.
- [5] Bapat, M. S.; Singh, H.; Shukla, S. K.; Singh, P. P.; Vo, D. V. N.; Yadav, A.; Goyal, A.; Sharma, A.; Kumar, D. Evaluating Green Silver Nanoparticles as Prospective Biopesticides: An Environmental Standpoint. *Chemosphere.* **2022**, *286*, 131761.
- [6] Siegel, R. L.; Miller, K. D.; Fuchs, H. E.; Jemal, A. Cancer Statistics, 2021. *A Cancer J. Clin.* **2021**, *71*, 7–33.
- [7] Rawla, P. Epidemiology of Prostate Cancer. *World J. Oncol.* **2019**, *10*, 63–89.
- [8] Baskar, R.; Lee, K. A.; Yeo, R.; Yeoh, K. W. Cancer and Radiation Therapy: Current Advances and Future Directions. *Int. J. Med. Sci.* **2012**, *9*, 193–199.
- [9] Almalki, M. A.; Khalifa, A. Y. Silver Nanoparticles Synthesis from *Bacillus* sp KFU36 and Its Anticancer Effect in Breast Cancer MCF-7 Cells via Induction of Apoptotic Mechanism. *J. Photochem. Photobiol. B.* **2020**, *204*, 111786.
- [10] Gomathi, A. C.; Rajarathinam, S. X.; Sadiq, A. M.; Rajeshkumar, S. Anticancer Activity of Silver Nanoparticles Synthesized Using Aqueous Fruit Shell Extract of *Tamarindus Indica* on MCF-7 Human Breast Cancer Cell Line. *J. Drug. Deliv. Sci. Technol.* **2020**, *55*, 101376.
- [11] Das, P.; Dutta, T.; Manna, S.; Loganathan, S.; Basak, P. Facile Green Synthesis of Non-Genotoxic, Non-Hemolytic Organometallic Silver Nanoparticles Using Extract of Crushed, Wasted, and Spent Humulus Lupulus (Hops): Characterization, Anti-Bacterial, and Anti-Cancer Studies. *Environ. Res.* **2022**, *204*, 111962.
- [12] Varadavenkatesan, T.; Pai, S.; Vinayagam, R.; Selvaraj, R. Characterization of Silver Nano-Spheres Synthesized Using the Extract of *Arachis hypogaea* Nuts and Their Catalytic Potential to Degrade Dyes. *Mater. Chem. Phys.* **2021**, *272*, 125017.
- [13] Varadavenkatesan, T.; Selvaraj, R.; Vinayagam, R. Green Synthesis of Silver Nanoparticles Using *Thunbergia Grandiflora* Flower Extract and Its Catalytic Action in Reduction of Congo Red Dye. *Mater. Today Proc.* **2020**, *23*, 39–42.
- [14] Selvaraj, R.; Pai, S.; Murugesan, G.; Pandey, S.; Bhole, R.; Gonsalves, D.; Varadavenkatesan, T.; Vinayagam, R. Green Synthesis of Magnetic α -Fe₂O₃ Nanospheres Using *Bridelia Retusa* Leaf Extract for Fenton-like Degradation of Crystal Violet Dye. *Appl. Nanosci.* **2021**, *11*, 2227–2234.
- [15] Dutta, T.; Chowdhury, S. K.; Ghosh, N. N.; Chattopadhyay, A. P.; Das, M.; Mandal, V. Synthesis of Antimicrobial Silver Nanoparticles Using Fruit Extract of *Glycosmis Pentaphylla* and Its Theoretical Explanations. *J. Mol. Struct.* **2022**, *1247*, 131361.
- [16] Tehri, N.; Vashishth, A.; Gahlaut, A.; Hooda, V. Biosynthesis, Antimicrobial Spectra and Applications of Silver Nanoparticles: Current Progress and Future Prospects. *Nano-Met. Chem.* **2022**, *52*, 1–19.
- [17] Pachaiyappan, A.; Sadhasivam, G.; Kumar, M.; Muthuvel, A. Biomedical Potential of Astaxanthin from Novel Endophytic Pigment Producing Bacteria *Pontibacter korlensis* AG6. *Waste. Biomass. Valori.* **2021**, *12*, 2119–2129.
- [18] Azmi, S. N. H.; Al-Jassasi, B. M. H.; Al-Sawafi, H. M. S.; Al-Shukaili, S. H. G.; Rahman, N.; Nasir, M. Optimization for Synthesis of Silver Nanoparticles through Response Surface Methodology Using Leaf Extract of *Boswellia Sacra* and Its Application in Antimicrobial Activity. *Environ. Monit. Assess.* **2021**, *193*, 1–16.
- [19] EUCAST. Determination of Minimum Inhibitory Concentrations (MICs) of Antibacterial Agents by Broth Dilution. *Clin. Microbiol. Infect.* **2003**, *9*, 1–7.
- [20] Könen-Adı güzel, S.; Adı güzel, A. O.; Ay, H.; Alpdogan, S.; Şahin, N.; Çaputçu, A.; Ergene, R. S.; Gübür, H. M.; Tunçer, M.; Genotoxic, C. Antimicrobial and Antioxidant Properties of Gold Nanoparticles Synthesized by *Nocardia* sp. GTS18 Using Response Surface Methodology. *Mater. Res. Express.* **2018**, *5*, 115402.

- [21] Wiegand, I.; Hilpert, K.; Hancock, R. E. W. Agar and Broth Dilution Methods to Determine the Minimal Inhibitory Concentration (MIC) of Antimicrobial Substances. *Nat. Protoc.* **2008**, *3*, 163–175.
- [22] Crémet, L.; Corvec, S.; Batard, E.; Auger, M.; Lopez, I.; Pagniez, F.; Dauvergne, S.; Caroff, N. Comparison of Three Methods to Study Biofilm Formation by Clinical Strains of *Escherichia coli*. *Diagn. Microbiol. Infect. Dis.* **2013**, *75*, 252–255.
- [23] Akçaözöğlü, S.; Adıgüzel, A. O.; Akçaözöğlü, K.; Deveci, E. Ü.; Gönen, Ç. Investigation of the Bacterial Modified Waste PET Aggregate via *Bacillus safensis* to Enhance the Strength Properties of Mortars. *Constr. Build. Mater.* **2021**, *270*, 121828.
- [24] Singh, N. P.; McCoy, M. T.; Tice, R. R.; Schneider, E. L. A Simple Technique for Quantitation of Low Levels of DNA Damage in Individual Cells. *Exp. Cell. Res.* **1988**, *175*, 184–189.
- [25] Lee, K. C.; Lin, S. J.; Lin, C. H.; Tsai, C. S.; Lu, Y. J. Size Effect of Ag Nanoparticles on Surface Plasmon Resonance. *Surf. Coat. Technol.* **2008**, *202*, 5339–5342.
- [26] Salem, S. S.; El-Belely, E. F.; Niedbala, G.; Alnoman, M. M.; Hassan, S. E. D.; Eid, A. M.; Shaheen, T. I.; Elkesh, A.; Fouda, A. Bactericidal and in-Vitro Cytotoxic Efficacy of Silver Nanoparticles (Ag-NPs) Fabricated by Endophytic Actinomycetes and Their Use as Coating for the Textile Fabrics. *Nanomaterials*. **2020**, *10*, 2082.
- [27] Ajaz, S.; Ahmed, T.; Shahid, M.; Noman, M.; Shah, A. A.; Mehmood, M. A.; Abbas, A.; Cheema, A. I.; Iqbal, M. Z.; Li, B. Bioinspired Green Synthesis of Silver Nanoparticles by Using a Native *Bacillus* sp. Strain AW1-2: Characterization and Antifungal Activity against *Colletotrichum Falcatum* Went. *Enzyme Microb. Technol.* **2021**, *144*, 109745.
- [28] Yari, T.; Vaghari, H.; Adibpour, M.; Jafarizadeh-Malmiri, H.; Berenjian, A. Potential Application of *Aspergillus terreus*, as a Biofactory, in Extracellular Fabrication of Silver Nanoparticles. *Fuel*. **2022**, *308*, 122007.
- [29] Kawahara, T.; Izumikawa, M.; Otoguro, M.; Yamamura, H.; Hayakawa, M.; Takagi, M.; Shin-ya, K. Shin-ya, K. JBIR-94 and JBIR-125, Antioxidative Phenolic Compounds from *Streptomyces* sp. R56-07. *J. Nat. Prod.* **2012**, *75*, 107–110.
- [30] Das, R.; Romi, W.; Das, R.; Sharma, H. K.; Thakur, D. Antimicrobial Potentiality of Actinobacteria Isolated from Two Microbiologically Unexplored Forest Ecosystems of Northeast India. *BMC Microbiol.* **2018**, *18*, 1–16.
- [31] Javaid, A.; Oloketuyi, S. F.; Khan, M. M.; Khan, F. Diversity of Bacterial Synthesis of Silver Nanoparticles. *BioNanoSci.* **2018**, *8*, 43–59.
- [32] Rahman, S.; Rahman, L.; Khalil, A. T.; Ali, N.; Zia, D.; Ali, M.; Shinwari, Z. K. Endophyte-Mediated Synthesis of Silver Nanoparticles and Their Biological Applications. *Appl. Microbiol. Biotechnol.* **2019**, *103*, 2551–2569.
- [33] Sivasankar, P.; Seedeve, P.; Poongodi, S.; Sivakumar, M.; Murugan, T.; Sivakumar, L.; Sivakumar, K.; Balasubramanian, T. Characterization, Antimicrobial and Antioxidant Property of Exopolysaccharide Mediated Silver Nanoparticles Synthesized by *Streptomyces violaceus* MM72. *Carbohydr. Polym.* **2018**, *181*, 752–759.
- [34] Goel, N.; Ahmad, R.; Singh, R.; Sood, S.; Khare, S. K. Biologically Synthesized Silver Nanoparticles by *Streptomyces* sp. EMB24 Extracts Used against the Drug-Resistant Bacteria. *Bioresour. Technol. Rep* **2021**, *15*, 100753.
- [35] Alam, A.; Tanveer, F.; Khalil, A. T.; Zohra, T.; Khamlich, S.; Alam, M. M.; Salman, M.; Ikram, A.; Shinwari, Z. K.; Maaza, M. Silver Nanoparticles Biosynthesized from Secondary Metabolite Producing Marine Actinobacteria and Evaluation of Their Biomedical Potential. *Antonie Leeuwenhoek*. **2021**, *114*, 1–20.
- [36] Sanjivkumar, M.; Vaishnavi, R.; Neelakannan, M.; Kannan, D.; Silambarasan, T.; Immanuel, G. Investigation on Characterization and Biomedical Properties of Silver Nanoparticles Synthesized by an Actinobacterium *Streptomyces olivaceus* (MSU3). *Biocatal. Agric. Biotechnol.* **2019**, *17*, 151–159.
- [37] Dhanaraj, S.; Thirunavukkarasu, S.; John, H. A.; Pandian, S.; Salmen, S. H.; Chinnathambi, A.; Alharbi, S. A. Novel Marine *Nocardiopsis dassonvillei*-DS013 Mediated Silver Nanoparticles Characterization and Its Bactericidal Potential against Clinical Isolates. *Saudi J. Biol. Sci.* **2020**, *27*, 991–995.
- [38] Wypij, M.; Jędrzejewski, T.; Trzcińska-Wencel, J.; Ostrowski, M.; Rai, M.; Golińska, P. Green Synthesized Silver Nanoparticles: Antibacterial and Anticancer Activities, Biocompatibility, and Analyses of Surface-Attached Proteins. *Front. Microbiol.* **2021**, *12*, 888.
- [39] Bakhtiari-Sardari, A.; Mashreghi, M.; Eshghi, H.; Behnam-Rasouli, F.; Lashani, E.; Shahnavaz, B. Comparative Evaluation of Silver Nanoparticles Biosynthesis by Two Cold-Tolerant *Streptomyces* Strains and Their Biological Activities. *Biotechnol. Lett.* **2020**, *42*, 1985–1999.
- [40] Vanaja, M.; Annadurai, G. *Coleus Aromaticus* Leaf Extract Mediated Synthesis of Silver Nanoparticles and Its Bactericidal Activity. *Appl. Nanosci.* **2013**, *3*, 217–223.
- [41] Railean-Plugaru, V.; Pomastowski, P.; Wypij, M.; Szultka-Mlynska, M.; Rafinska, K.; Golinska, P.; Dahm, H.; Buszewski, B. Study of Silver Nanoparticles Synthesized by Acidophilic Strain of Actinobacteria Isolated from the of *Picea Sitchensis* Forest Soil. *J. Appl. Microbiol.* **2016**, *120*, 1250–1263.
- [42] Huq, M. Biogenic Silver Nanoparticles Synthesized by *Lysinibacillus xylanilyticus* MAHUQ-40 to Control Antibiotic-Resistant Human Pathogens *Vibrio parahaemolyticus* and *Salmonella Typhimurium*. *Front. Bioeng. Biotechnol.* **2020**, *8*, 1407.
- [43] Hamed, A. A.; Kabary, H.; Khedr, M.; Emam, A. N. Antimicrobial and Cytotoxic Activity of Extracellular Green-Synthesized Silver Nanoparticles by Two Marine-Derived Actinomycete. *RSC Adv.* **2020**, *10*, 10361–10367.
- [44] Bahrami-Teimoori, B.; Pourianfar, H. R.; Akhlaghi, M.; Tanhaeian, A.; Rezayi, M. Biosynthesis and Antibiotic Activity of Silver Nanoparticles Using Different Sources: Glass Industrial Sewage-Adapted *Bacillus* sp. and Herbaceous *Amaranthus* sp. *Biotechnol. Appl. Biochem.* **2019**, *66*, 900–910.
- [45] Mohanta, Y. K.; Behera, S. K. Characterization and Antimicrobial Activity of Silver Nanoparticles by *Streptomyces* sp. SS2. *Bioprocess Biosyst. Eng.* **2014**, *37*, 2263–2269.
- [46] Anasane, N.; Golińska, P.; Wypij, M.; Rathod, D.; Dahm, H.; Rai, M. Acidophilic Actinobacteria Synthesized Silver Nanoparticles Showed Remarkable Activity against Fungi-Causing Superficial Mycoses in Humans. *Mycoses*. **2016**, *59*, 157–166.
- [47] Çelik, T.; Adıgüzel, S. K.; Adıgüzel, A. O. Synthesis of Silver Nanoparticles by *Kribbella Turkmenica* 16K104, Their Characterization. *Antimicrob. Prop. Genotox. Potent.* **2021**, *11*, 3138–3151.
- [48] Aygün, A.; Özdemir, S.; Gülcan, M.; Yalçın, M. S.; Uçar, M.; Şen, F. Characterization and Antioxidant-Antimicrobial Activity of Silver Nanoparticles Synthesized Using *Punica Granatum* Extract. *Int. J. Environ. Sci. Technol.* **2022**, *19*, 2781–2788.
- [49] Ulagesan, S.; Nam, T. J.; Choi, Y. H. Biogenic Preparation and Characterization of *Pyropia Yezoensis* Silver Nanoparticles (Py AgNPs) and Their Antibacterial Activity against *Pseudomonas aeruginosa*. *Bioprocess Biosyst. Eng.* **2021**, *44*, 443–452.
- [50] Gopu, M.; Kumar, P.; Selvakumar, T.; Senthilkumar, B.; Sudhakar, C.; Govarthanan, M.; Kumar, R. S.; Selvam, K. Green Biomimetic Silver Nanoparticles Utilizing the Red Algae *Amphiroa Rigida* and Its Potent Antibacterial, Cytotoxicity and Larvicidal Efficiency. *Bioprocess Biosyst. Eng.* **2021**, *44*, 217–223.
- [51] Elbahnasawy, M. A.; Shehabeldine, A. M.; Khattab, A. M.; Amin, B. H.; Hashem, A. H. Green Biosynthesis of Silver Nanoparticles Using Novel Endophytic *Rothia endophytica*: Characterization and Anticandidal Activity. *J. Drug. Deliv. Sci. Technol.* **2021**, *62*, 102401.

- [52] Jalilian, F.; Chahardoli, A.; Sadrjavadi, K.; Fattahi, A.; Shokoohinia, Y. Green Synthesized Silver Nanoparticle from *Allium Ampeloprasum* Aqueous Extract: Characterization, Antioxidant Activities, Antibacterial and Cytotoxicity Effects. *Adv. Powder. Technol.* **2020**, *31*, 1323–1332.
- [53] Khan, M.; Shaik, M. R.; Khan, S. T.; Adil, S. F.; Kuniyil, M.; Khan, M.; Al-Warthan, A. A.; Siddiqui, M. R. H., Nawaz Tahir, M. Enhanced Antimicrobial Activity of Biofunctionalized Zirconia Nanoparticles. *ACS Omega.* **2020**, *5*, 1987–1996.
- [54] Swolana, D.; Kępa, M.; Idzik, D.; Dziedzic, A.; Kabała-Dzik, A.; Wąsik, T. J.; Wojtyczka, R. D. The Antibacterial Effect of Silver Nanoparticles on *Staphylococcus epidermidis* Strains with Different Biofilm-Forming Ability. *Nanomaterials.* **2020**, *10*, 1010.
- [55] Kumar, S.; Basumatary, I. B.; Sudhani, H. P.; Bajpai, V. K.; Chen, L.; Shukla, S.; Mukherjee, A. Plant Extract Mediated Silver Nanoparticles and Their Applications as Antimicrobials and in Sustainable Food Packaging: A State-Of-the-Art Review. *Trends Food Sci. Technol.* **2021**, *112*, 651–666.
- [56] Shanthi, S.; Jayaseelan, B. D.; Velusamy, P.; Vijayakumar, S.; Chih, C. T.; Vaseeharan, B. Biosynthesis of Silver Nanoparticles Using a Probiotic *Bacillus licheniformis* Dabhl and Their Antibiofilm Activity and Toxicity Effects in *Ceriodaphnia Cornuta*. *Microb. Pathog.* **2016**, *93*, 70–77.
- [57] Rolim, W. R.; Lamilla, C.; Pieretti, J. C.; Díaz, M.; Tortella, G. R.; Diez, M. C.; Barrientos, L.; Seabra, A. B.; Rubilar, O. Comparison of Antibacterial and Antibiofilm Activities of Biologically Synthesized Silver Nanoparticles against Several Bacterial Strains of. *Energ. Ecol. Environ.* **2019**, *4*, 143–159.
- [58] Mohanta, Y. K.; Biswas, K.; Jena, S. K.; Hashem, A.; Abd Allah, E. F.; Mohanta, T. K. Anti-Biofilm and Antibacterial Activities of Silver Nanoparticles Synthesized by the Reducing Activity of Phytoconstituents Present in the Indian Medicinal Plants. *Front. Microbiol.* **2020**, *11*, 1143.
- [59] Padalia, H.; Chanda, S. Synthesis of Silver Nanoparticles Using *Ziziphus Nummularia* Leaf Extract and Evaluation of Their Antimicrobial, Antioxidant, Cytotoxic and Genotoxic Potential (4-in-1 System). *Artif. Cells. Nanomed. Biotechnol.* **2021**, *49*, 354–366.
- [60] Zamanpour, N.; Esmaeily, A. M.; Mashreghi, M.; Shahnavaz, B.; Sharifmoghadam, M. R.; Kompany, A. Application of a Marine Luminescent *Vibrio* sp. B4L for Biosynthesis of Silver Nanoparticles with Unique Characteristics, Biochemical Properties, Antibacterial and Antibiofilm Activities. *Bioorg. Chem.* **2021**, *114*, 105102.
- [61] Singh, P.; Pandit, S.; Jers, C.; Joshi, A. S.; Garnaes, J.; Mijakovic, I. Silver Nanoparticles Produced from *Cedecea* sp. Exhibit Antibiofilm Activity and Remarkable Stability. *Sci. Rep* **2021**, *11*, 1–13.
- [62] Qayyum, S.; Oves, M.; Khan, A. U. Obliteration of Bacterial Growth and Biofilm through ROS Generation by Facilely Synthesized Green Silver Nanoparticles. *PLOS One.* **2017**, *12*, e0181363.
- [63] Mousavi-Khattat, M.; Keyhanfar, M.; Razmjou, A. A Comparative Study of Stability, Antioxidant, DNA Cleavage and Antibacterial Activities of Green and Chemically Synthesized Silver Nanoparticles. *Artif. Cells Nanomed. Biotechnol.* **2018**, *46*, 1022–1031.
- [64] Gulbagca, F.; Ozdemir, S.; Gulcan, M.; Sen, F. Synthesis and Characterization of Rosa Canina-Mediated Biogenic Silver Nanoparticles for anti-Oxidant, Antibacterial, Antifungal, and DNA Cleavage Activities. *Heliyon.* **2019**, *5*, e02980.
- [65] Aygün, A.; Ozdemir, S.; Gülcan, M.; Cellat, K.; Şen, F. Synthesis and Characterization of Reishi Mushroom-Mediated Green Synthesis of Silver Nanoparticles for the Biochemical Applications. *J. Pharm. Biomed. Anal.* **2020**, *178*, 112970.